Annals of Biomedical Engineering, Vol. 39, No. 6, June 2011 *(© 2011)* pp. 1728–1735
DOI: 10.1007/s10439-011-0261-1

Whole-Body Cerenkov Luminescence Tomography with the Finite Element SP_3 Method

JIANGHONG ZHONG, JIE TIAN, XIN YANG, and CHENGHU QIN

Medical Image Processing Group, Institute of Automation, Chinese Academy of Sciences, 95 Zhongguancun East Road, Haidian Dist., Beijing 100190, People's Republic of China

(Received 8 November 2010; accepted 24 January 2011; published online 8 February 2011)

Associate Editor Jing Bai oversaw the review of this article.

Abstract—Generation of an accurate Cerenkov luminescence imaging model is a current issue of nuclear tomography with optical techniques. The article takes a pro-active approach toward whole-body Cerenkov luminescence tomography. The finite element framework employs the equation of radiative transfer via the third-order simplified spherical harmonics approximation to model Cerenkov photon propagation in a small animal. After this forward model is performed on a digital mouse with optical property heterogeneity and compared with the Monte Carlo method, we investigated the whole body reconstruction algorithm along a regularization path via coordinate descent. The endpoint of the follow-up study is the *in vivo* application, which provides three-dimensional biodistribution of the radiotracer uptake in the mouse from measured partial boundary currents. The combination of the forward and inverse model with elastic-net penalties is not only validated by numerical simulation, but it also effectively demonstrates *in vivo* imaging in small animals. Our exact reconstruction method enables optical molecular imaging to best utilize Cerenkov radiation emission from the decay of medical isotopes in tissues.

Keywords—Cerenkov, Mathematical model, Light propagation in tissues, Tomography, Molecular imaging.

INTRODUCTION

Whole-body Cerenkov tomographic imaging provides a new molecular imaging strategy to image radionuclides *in vivo* in a cost-effective and timely manner.[13] Radiotracers are generally imaged with nuclear imaging modalities such as positron emission tomography (PET) and single photon emission computed tomography (SPECT). An optical imaging modality has been recently discovered to be able to image medical isotopes such as ^{18}F, ^{131}I, and ^{225}Ac *in vivo* in small animals utilizing Vavilov–Cerenkov radiation (VCR).[8–11,16–18] VCR is generated during the initial decay process before the annihilation event and emits a continuum of ultraviolet and visible light. More than a low-cost PET or SPECT alternative, utilization of Cerenkov luminescence and tomographic techniques breaks the limitation of pure optical approaches by the lack of clinically approved targeted agents. Cerenkov luminescence tomography (CLT) with functional and anatomical information opens a door for optical imaging to the clinics using hand-held probes and radioactive contrast agents.[13,19]

Image quality of optical tomography has relied mostly on the model-based reconstruction method.[1] The forward model to describe light propagation in turbid media is essential for optical tomography. Radiation transport equation (RTE) has been used as a standard forward model and is considered as an equivalent to the numerical Monte Carlo (MC) method. It is difficult to solve RTE directly, which is often approximated by the diffusion equation (DE) to save on computational costs. The Cerenkov radiation spectrum is weighted toward blue bands of the electromagnetic spectrum.[4] The large absorption coefficients at these wavelengths make the diffusion approximation as a light propagation model less accurate. The DE fails to work, especially in some regions with a highly heterogeneous optical background and small geometries.[6] Tomographic reconstruction will subsequently lead to erroneous imaging of the radiopharmaceutical. The current spherical harmonics (SP_N) approximation can generate a more transport-like solution to RTE than DE, of which the third-order simplified spherical harmonics (SP_3) approximation retains this feature with a minimal cost. Although the SP_N forward model in fluorescence or

Address correspondence to Jie Tian, Medical Image Processing Group, Institute of Automation, Chinese Academy of Sciences, 95 Zhongguancun East Road, Haidian Dist., Beijing 100190, People's Republic of China. Electronic mail: tian@ieee.org

bioluminescence tomography has been reported,[5,12] further efforts to study the performance of this approximation approach in CLT are needed.

In this study, the performance of the SP_3 model-based CLT method is fully investigated. We first provide a comparative demonstration with both of the finite element SP_3 method and MC simulations. Considering that there are relatively more diagnostic or therapeutic radiotracers in a very small targeted zone as compared with the whole body sparse biodistribution is the result. In another case, there is also a target region with fewer radionuclides relative to other normal tissues. Hence, we applied elastic-net penalties[3] into the whole body reconstruction based on the SP_3 forward model. Further validation of the CLT framework, including the forward and inverse models, is illustrated in small animal practice. Results of numerical simulations and *in vivo* experiments reveal that whole-body CLT with the SP_3 method can provide an accurate three-dimensional (3D) approach to optical imaging with radionuclides.

MATERIALS AND METHODS

Radionuclide

^{18}F-FDG was kindly provided as a generous gift from the Department of Nuclear Medicine, Beijing Union Medical College Hospital.

Digimouse

The digimouse (http://www.mosetm.net) was generated as a 3D whole body mouse atlas with $0.1 \times 0.1 \times 0.2$ mm^3 voxels and a matrix size of $384 \times 600 \times 480$ using micro-computed tomography (micro-CT) data. Here, we selected part of the digimouse data along the z axis from the 121st to the 320th slice to carry out MC simulations and CLT reconstruction. It was meshed into triangular facets in MC simulations, including the heart (9002 points, 18000 faces), lungs (15002 points, 30000 faces), liver (15002 points, 30000 faces), stomach (15028 points, 30052 faces), and muscle (30002 points, 59998 faces).

Phantom

We have designed a combination of four materials into the phantom (Fig. 1a) to simulate the real environment of small animals, the abdomen, including muscle, heart, lungs, and bone. Optical parameters of the phantom are shown in Table 1, which were measured by the TCSPC system.[20] The phantom is a cylinder (diameter, 30 mm; height, 30 mm), containing a small cylinder hole (diameter, 2 mm; height, 3 mm), as shown in Figs. 1b and 1c. The green hole was filled with a solution containing a total of 4.4 MBq ^{18}F-FDG.

Mouse Model

The healthy, female Nu/Nu nude mice utilized in the experiment were purchased from the Department of Laboratory Animal Science, Peking University Health Science Centre. Animal experimentation was conducted under approved research protocols of the Institutional Animal Care and Use Committee. All animal procedures were performed under anesthesia by inhalation of 2% isoflurane delivered via medical air.

Computer

In vivo imaging system control and image processing were performed on a personal computer with Intel Core^{TM} 2 Duo Processor 2.33 GHz and 3 GB RAM. The forward and inverse models for CLT using the SP_3 method were written in C++.

Computed Tomography

Our micro-CT system provides 3D anatomical information in accordance with the same methods and instrument parameters as described[21] for the mouse micro-CT studies.

The mouse was injected with 0.20 mL of Fenestra LC (Advanced Research Technologies Inc., QC, Canada) and 11.10 MBq of ^{18}F-FDG via the tail vein. Micro-CT images with a size of $400 \times 400 \times 560$ were recorded half an hour after injection. The voxel of micro-CT data was a 0.15-mm cubed volume.

Optical Imaging

Optical imaging was performed with an *in vivo* molecular imaging system developed by our group. The CCD camera (Princeton Instruments VersArray 1300B, Roper Scientific, Trenton, NJ) has 1340×1300 pixels with 20×20 μm^2 sized pixels. Low readout and binning noise makes this camera ideal for Cerenkov optical imaging. The optical imaging system has a dark room that can block both external lights and internal high-energy radiation. The optical system was calibrated with an integrating sphere (USS-1200V-LL Low-Light Uniform Source, Labsphere, North Sutton, NH), according to the quantitative calibration formula: $S = (2.09p \cdot t^{-1} + 10.89) \times 10^{-10}$ W mm^{-3}, where S is source energy density, p is the 16 bits CCD pixel intensity value, and t is the exposure time with units of s.

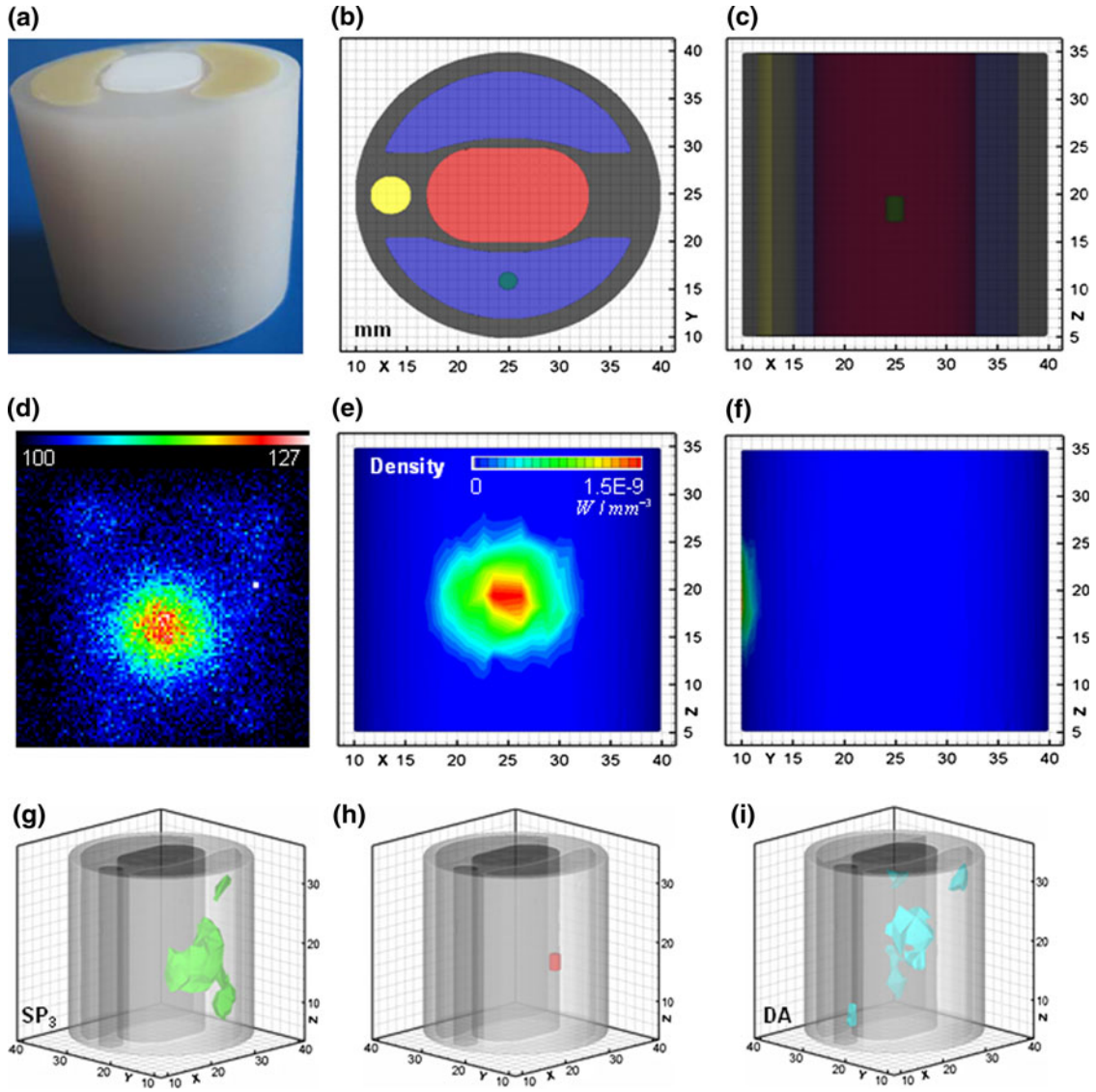

FIGURE 1. Physical experiment on the phantom. (a–c) The schematic of materials and the internal structure (gray muscle, red heart, blue lungs, yellow bone, and green cylinder hole); (d) the Cerenkov luminescence image with the maximum light intensity value of 127 for all pixels, except for an outlier; (e, f) the measured optical energy density distribution on the surface of the finite element mesh, of which the peak value is 1.5 Nano-W mm^{-3}; (g, i) iso-surfaces of the reconstructed source, based on the SP_3 and DA model, respectively; (h) the actual source location with a red colour as a reference. A millimeter (mm) is a unit of length in (b), (c), (e–i).

TABLE 1. Optical parameters of the phantom with units of 10^{-2} mm^{-1}.

Material	Heart	Lung	Muscle	Bone
Absorption coefficient	1.1	2.3	0.7	0.1
Reduced scattering coefficient	109.6	200.0	103.1	6.0

Optical images were acquired (aperture number *f*, 2.8; binning value, 2; integration time, 180 s) at a quarter of an hour after micro-CT scanning. There was no optical filter because of very weak Cerenkov signals. A Cerenkov luminescence image was obtained after a 90° rotation of the turntable. We rotated the turntable 360° to have four luminescence images.

MC Simulation

We performed MC simulations using MOSE v2.1 (http://www.mosetm.net.) and the surface mesh of the partial digimouse.[15] Two point light sources were set at (18, 31, and 36 mm) and (21, 42, and 53 mm), respectively, with a total energy of 1×10^{-9} W and 1×10^{6} photons. The tissue-optics parameters (Table 2) were set as the weighted values in order to simulate the *in vivo* CLT situation without optical filters.

TABLE 2. Optical parameters of the nude mouse with units of 10^{-2} mm^{-1}.[12]

Material	Heart	Lung	Liver	Stomach	Muscle	Kidney	Bladder	Bone
Absorption coefficient	2.2	7.1	12.8	3.5	3.2	1.0	68.4	0.24
Reduced scattering coefficient	112.9	230.5	64.6	148.0	58.6	83.0	139.0	93.5

Forward Model

When exploring the application of Cerenkov luminescence in optical tomography, higher-order approximations to the RTE are required. We derived the governed matrix equation from SP_3 approximation,[6] utilizing the finite element discretization[12]:

$$\begin{bmatrix} M_{11} & M_{12} \\ M_{21} & M_{22} \end{bmatrix} \begin{Bmatrix} Q_1 \\ Q_2 \end{Bmatrix} = [M] \begin{Bmatrix} Q_1 \\ Q_2 \end{Bmatrix} = \begin{bmatrix} F & 0 \\ 0 & F \end{bmatrix} \begin{Bmatrix} S \\ -2S/3 \end{Bmatrix}, \tag{1}$$

where M and F are the coefficient; and Q_1 and Q_2 are the optical energy density in W mm^{-3}. After computing the approximate generalized inverse of M_{11} and the Schur complement[2] with the singular value decomposition (SVD) method, the inverse of M is matrix M^+ $\left(M^+ = \begin{bmatrix} P_{11} & P_{12} \\ P_{21} & P_{22} \end{bmatrix}\right)$. The linear relationship between the boundary photon flux density J on the surface in units of W mm^{-3} and the source density S is defined as

$$J = [a(P_{11} - 2P_{12}/3) + b(P_{21} - 2P_{22}/3)]FS = AS, \tag{2}$$

where a and b are the constants[8] and A is an $N \times M$ coefficient matrix.

Inverse Model

The inverse model for whole body CLT reconstruction is defined as an optimization problem:

$$\min_{S \in R^M} \left[\sum_{i=1}^{N} (J_i - A_i S)^2/(2N) + cP_d(S) \right]. \tag{3}$$

Here, A_i is the ith row of A; J_i is the ith element of J; c is the regulation parameter $(N \cdot c \cdot d = 2 \times 10^{-3} \max_i ||\langle A_i, J \rangle||)$; $P_d(S) = (0.5(1 - d)) \cdot ||S||_2 + d \cdot ||S||_1$; and d is a constant between 0 and 1. We set $d = 0.2$ in the article. The iterative formula of the jth unknown item S_j of S is

$$S_j = \frac{f\left(\sum_{i=1}^{N} A_{ij}(J_i - J_{ij})/N, c \cdot d\right)}{\sum_{i=1}^{N} A_{ij}^2 + c(1 - d)}, \tag{4}$$

where f is the soft-thresholding operator,[3] and J_{ij} is the fitted value excluding the contribution from A_{ij}. A maximum of 50 and a terminate threshold of 1×10^{-3} outer-loop iterations were used in numerical simulations and physical experiments.

RESULTS

Forward Simulation

Figure 2 shows two spherical light sources with a 1-mm radius inside the same partial digimouse as the one used in MC simulations and the tetrahedral mesh. The shortest distance from every spherical center to the surface was 3.5 mm. We cut down four slices (Slice 1: $x = 23$ mm; Slice 2: $y = 31$ mm; Slice 3: $z = 36$ mm; Slice 4: $z = 53$ mm) in order to display the light source (Fig. 2a) and measure energy densities on the surface derived from these two methods at the same points. This finite element mesh including 3494 nodes, 36304 triangles, and 17690 tetrahedrons was used as the input for the SP_3 model. The optical properties parameters were set the same in both SP_3 and MC simulations. Figure 3 is the experimental results of the forward simulation. The MC simulation data (Fig. 3a: Peak value was 6.1×10^{-12} W mm^{-3}) and the solution of SP_3 approximation (Fig. 3b: Peak value was 4.0×10^{-12} W mm^{-3}) had similar optical distributions on the surface. We recorded the energy densities at all boundary points along those four slices (Fig. 4). Although the magnitude of each curve was not the same, their distributions derived from the two methods were consistent. These results proved that the forward model via SP_3 approximation could yield a transport-like solution as compared to the MC method.

Numerical Reconstruction

The feasibility of inverse CLT reconstruction was validated on the basis of the SP_3 forward model. Figure 5 illustrates the numerical results inversely traced back from light distribution on the surface through MC simulation (Fig. 3a). A is an ill-posed coefficient matrix with a size of 926×17690 in the last reconstruction procedure. Two orthogonal slices were extracted through each light source center to show the reconstructed distribution in the same digimouse. We selected the geometric center of the tetrahedron with the maximum flux rate value of the targeted area as the recovered center to quantify the reconstruction distance error

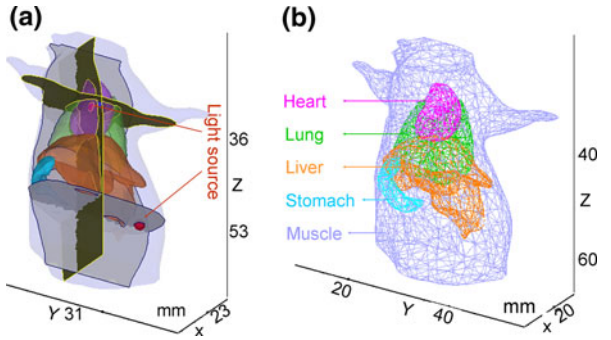

FIGURE 2. Schematic of the digimouse used by the forward SP_3 model. Two spherical light sources with a radius 1 mm inside the same partial digimouse as the one used in the MC simulations (a) and the tetrahedral mesh (b).

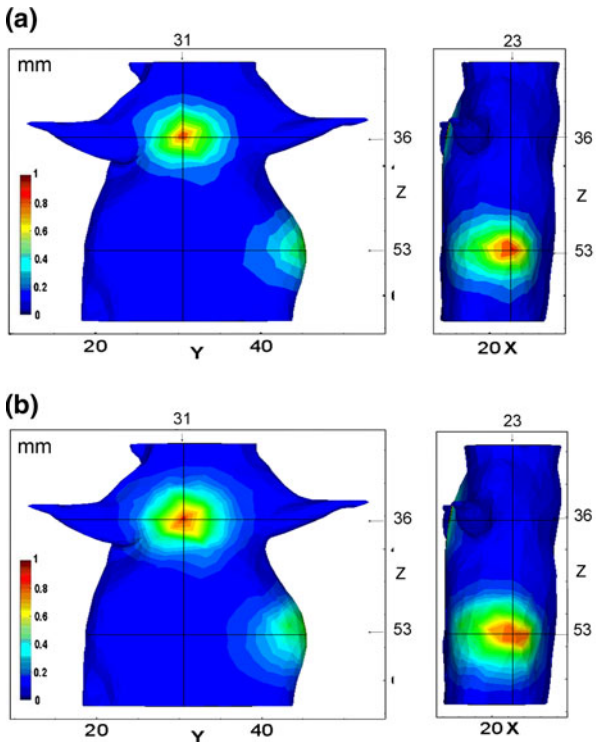

FIGURE 3. Optical energy density distribution on the surface derived from the forward simulation. (a) The MC simulation data. (b) The solution of SP_3 approximation.

between the light source center and the recovered one. Here, the distance between two points was calculated in the L_2 norm. The recovered distance errors were 2.1 and 2.6 mm for these two sources. The reconstruction depth became a major contributor to the reconstruction error (Fig. 5). In other words, quantitative reconstruction could be achieved using the proposed method.

Phantom Experiment

The Cerenkov luminescence image (Fig. 1d) of the phantom was collected by our optical system (aperture number *f*, 2.8; binning value, 2; integration time, 60 s). With the help of micro-CT system, the fused volume data (size, $500 \times 500 \times 200$; element, $0.1 \times 0.1 \times 0.2$ mm^3) were discreted into a finite element mesh of 4399 nodes, 44774 triangles, and 21598 tetrahedrons. The mesh is displayed with the measured photon density in Figs. 1e and 1f. Cerenkov luminescence tomography (CLT) reconstruction was performed on the diffusion approximation[1] (DA) and SP_3 forward models, using the same inverse algorithm and parameters in the article. The reconstructed iso-surfaces are shown in Figs. 1g and 1i. Table 3 also gives the comparison of CLT reconstruction results between SP_3 and DA forward models in the physical phantom case. It took longer time to generate the stiffness matrix A for Eq. (2) ($J = AS$) with the SP_3 forward model than that based on the DA model. The minimum distance between the reconstruction center and the cylinder hole was 0.2 mm using the proposed method, which is much smaller than 5.7 mm derived from the DA model. Light source position is fixed and definite, which enhances the credibility of this physical experiment. These results prove that the SP_3 forward model can more accurately simulate propagation of light in biological tissues, especially with a complex boundary.

In Vivo Application

Our approach to CLT was performed during *in vivo* application with ^{18}F-FDG, as shown in Fig. 6. There was only one face emitting Cerenkov photons where light energy was strong enough to be detected by the camera, even though the turntable was rotated 360° (Fig. 6a). The optical signal was near the bladder (Fig. 6b). The mouse was discredited into the tetrahedral mesh as the input of the SP_3 model, including 3555 nodes, 38115 triangles, and 18690 tetrahedrons. The recovered center with the maximum light intensity of 4.4×10^{-12} W mm^{-3} was inside the bladder (Figs. 6c, 6d). A is an ill-posed coefficient matrix with a size of 737×18690 in the last reconstruction procedure. If the bladder was assumed as the only homogeneous light source because of its FDG uptaking capacity, we can quantitatively evaluate the accuracy of the reconstruction position. The geometric center of the bladder could be used as the true light center with the micro-CT information's aid. Thus, the recovered distance error of 2.3 mm was obtained.

DISCUSSION

We have presented a finite element SP_3 approach for CLT in localizing the *in vivo* medical isotopes uptake. In theory, the standard SP_3 method can handle photon

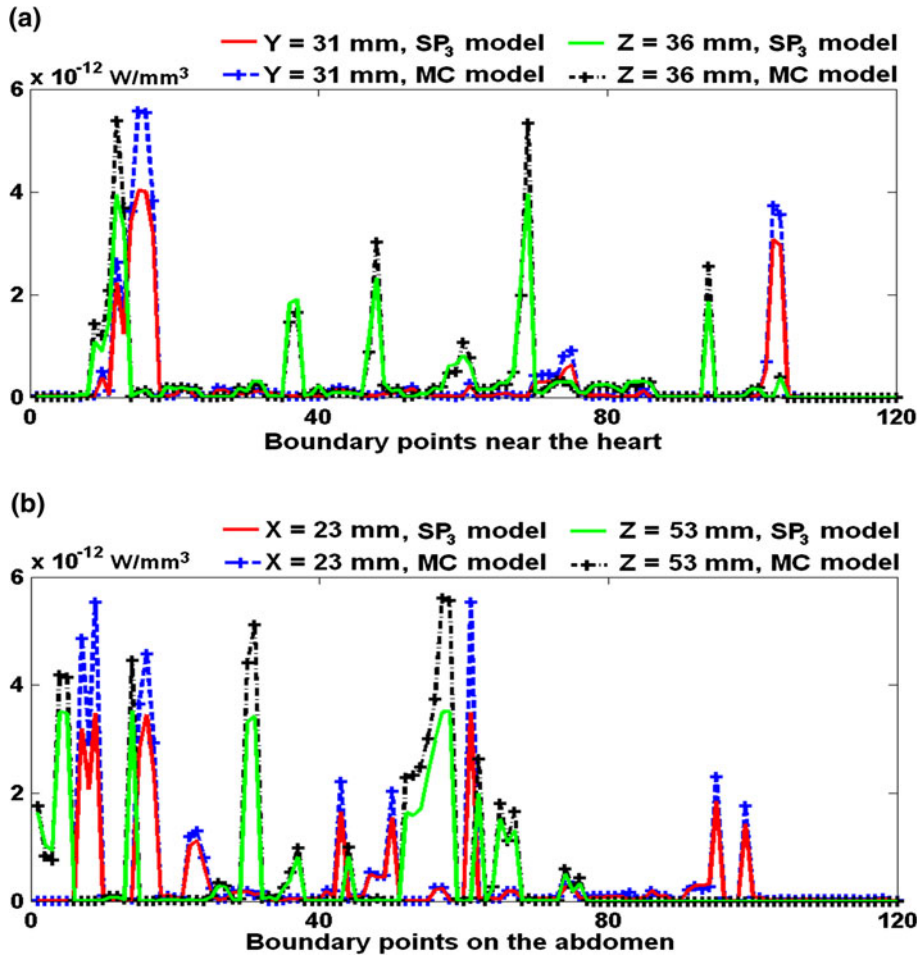

FIGURE 4. The energy densities at all boundary points along those four slices from both SP_3 approximation and MC simulations. (a) Light intensities on the boundary of slices $y = 31$ mm and $z = 36$ mm respectively. (b) Light intensities on the boundary of slices $x = 23$ mm and $z = 53$ mm respectively.

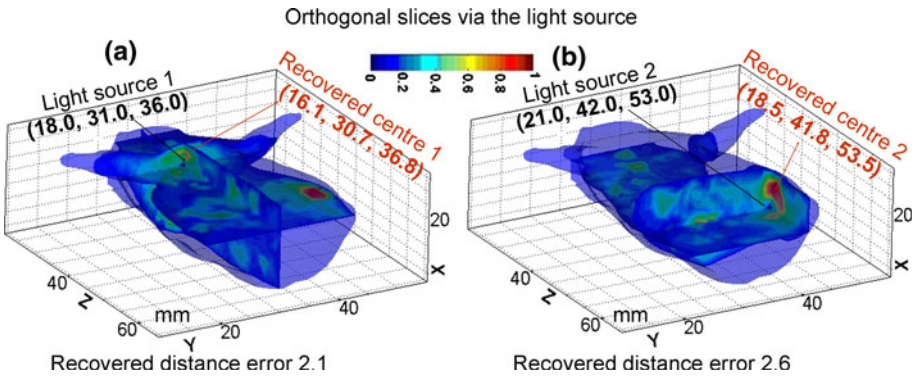

FIGURE 5. Numeric results of CLT reconstruction inversely from surfacial photon distribution via the MC simulations.

transport problems in complex media. It was able to be applied to model the Cerenkov electromagnetic spectrum, which is weighted to ultraviolet and blue bands. Taking into account that the coefficient matrix derived from the high-ordered differential and integral equation is ill-conditioned in the forward model, we adopted the Schur inversion lemma and SVD method in the finite element framework. Simulation results for the short wavelength were proven to be consistent with the MC method. Furthermore, the proposed CLT method was applied into physical experiments after numerical simulation. Quantitatively

optical reconstruction was completed on basis of SP_3 approximation solutions. Thus, it is worthwhile to complete this basic study for the CLT problem with the SP_3 approximation approach.

Our first observation is the impact of large absorption coefficients on the light propagation model. This was illustrated in Fig. 3 (the optical energy distribution on the surface in the chest was stronger than that in the abdomen) and Fig. 5 (the reconstructed optical energy distribution in the chest was weaker than that in the abdomen). In fact, the shortest distance from a different light source center to the surface is the same. The former light source was implanted within the heart, while the other was just surrounded by muscle.

TABLE 3. Comparisons of CLT reconstruction results using SP_3 and DA forward models in the physical phantom case.

Forward model	SP_3	DA
Time of generating matrix *A* (s)	13050	7190
Time of inverse reconstruction (s)	940	720
Maximum density (Nano-W mm^{-3})	44.6	38.0
Reconstructed center (mm)	(25.6, 15.0, 20.2)	(21.5, 15.0, 24.5)
Minimum distance from the hole (mm)	0.2	5.7

The finite element SP_3 method can characterize this difference to achieve the equivalent level with MC simulations when diffusion approximation is no longer applicable.

Our second observation concerns the impact of the physical position on the CLT reconstruction error. The absorption and scattering of light in tissues will aggravate the ill-posedness of the optical reconstruction. The error depth of Cerenkov optical tomography would increase with the deepening of the actual light source. The distance errors between the reconstructed center and the actual center in the simulations will be 0.9 mm (Fig. 5a) and 0.5 mm (Fig. 5b) if we do not take into account the depth of the *x* axis. This error would also be reduced to less than 1.1 mm in the mouse (Fig. 6) if we do not calculate the depth of the *y* axis. Although the surface light intensity was the same, the anatomical position and intensity of light may be different. Therefore, the space accuracy of 3D tomography imaging has been greatly affected by depth. Mathematically, it is still difficult to find a globally optimal solution to the ill-posed problem. How to obtain the solution to comprehensively model the radionuclide uptake and transport with optical techniques will be a more difficult mathematical problem to solve.

In addition, optical imaging technology has been widely applied to the pre-clinical fields, mainly based on fluorescence molecular imaging (FMI) and

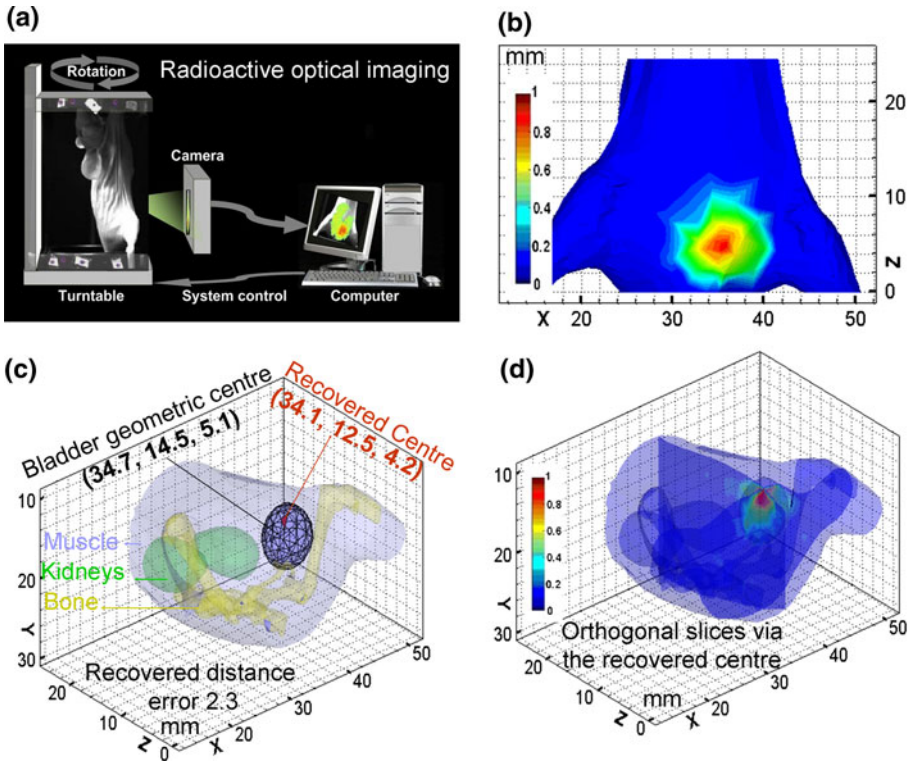

FIGURE 6. ***In vivo*** **application of whole-body CLT via finite element SP_3 approximation with ^{18}F-FDG.**

bioluminescence imaging (BLI). CLI is a new approach for optical imaging, using the isotope labeling technology. The biggest difference between FMI/BLI and CLI is from their molecular probes. One advantage of CLI is that molecular probes have good biocompatibility and permeability, with easer operation. Therefore, CLI may be a tool so as to observe the *in vivo* interaction between drugs and tumors, without changing the biological activity of drug molecules.

CONCLUSION

Improvement of mathematical model promotes the quality of optical tomography imaging, without any supernumerary operation on the molecular probes. The SP_3 method achieves a transport-like and accurate solution for modeling Cerenkov light propagation in biological tissues. Whole-body tomographic imaging of small animals with VCR could be performed, even if highly vascularized tissues with large absorption coefficients, e.g., bladder, liver, heart, and kidneys and their tissue vicinities, were imaged. Further, the proposed CLT technique with the radiotracer may open a door to the optical tomography clinic.

ACKNOWLEDGMENTS

This article is supported by the National Basic Research Program of China (973 Program) under Grant No. 2011CB707700, the Knowledge Innovation Project of the Chinese Academy of Sciences under Grant No. KGCX2-YW-907, the Program for Changjiang Scholars and Innovative Research Team in University of Ministry of Education (PCSIRT) under Grant No. IRT0645, the Hundred Talents Program of the Chinese Academy of Sciences, the National Natural Science Foundation of China under Grant Nos. 81027002, 81071205, and the Science and Technology Key Project of Beijing Municipal Education Commission under Grant No. KZ200910005005.

REFERENCES

[1]Arridge, S. R., and J. C. Schotland. Optical tomography: forward and inverse problems. *Inverse Probl.* 25:123010, 2009.

[2]Fortmann, T. E. A matrix inversion identity. *IEEE. Trans. Autom. Control* AC-15:599, 1970.

[3]Friedman, J. H., T. Hastie, and R. Tibshirani. Regularization paths for generalized linear models via coordinate descent. *J. Stat. Softw.* 33:1–22, 2010.

[4]Jelley, J. V. Cerenkov radiation and its application. *Br. J. Appl. Phys.* 6:227–232, 1955.

[5]Klose, A. D., and B. J. Beattie. Bioluminescence tomography with SP3 equations. In: OSA Topical Meetings: Biomedical Optics, St. Petersburg, FL, USA, March 15–20, BMC8, 2008.

[6]Klose, A. D., and E. W. Larsen. Light transport in biological tissue based on the simplified spherical harmonics equations. *J. Comput. Phys.* 220:441–470, 2006.

[7]Li, C., G. S. Mitchell, and S. R. Cherry. Cerenkov luminescence tomography for small animal imaging. *Opt. Lett.* 35:1109–1111, 2010.

[8]Liu, K., Y. Lu, J. Tian, C. Qin, X. Yang, S. Zhu, X. Yang, Q. Gao, and D. Han. Evaluation of the simplified spherical harmonics approximation in bioluminescence tomography through heterogeneous mouse models. *Opt. Express.* 18:20988–21002, 2010.

[9]Liu, H., G. Ren, S. Liu, X. Zhang, L. Chen, P. Han, and Z. Cheng. Optical imaging of reporter gene expression using a positron-emission-tomography probe. *J. Biomed. Opt.* 15:060505, 2010.

[10]Liu, H. G., G. Ren, Z. Miao, X. Zhang, X. Tang, P. Han, S. S. Gambhir, and Z. Cheng. Molecular optical imaging with radioactive probes. *PLoS One* 5:e9470, 2010.

[11]Liu, H., X. Zhang, B. Xing, P. Han, S. S. Gambhir, and Z. Cheng. Radiation luminescence excited quantum dots for in vivo multiplexed optical imaging. *Small* 6:1087–1091, 2010.

[12]Lu, Y., A. Douraghy, H. B. Machado, D. Stout, J. Tian, H. Herschman, and A. F. Chatziioannou. Spectrally-resolved bioluminescence tomography with the third-order simplified spherical harmonics approximation. *Phys. Med. Biol.* 54:6477–6493, 2009.

[13]Pysz, M. A., S. S. Gambhir, and J. K. Willmann. Molecular imaging: current status and emerging strategies. *Clin. Radiol.* 65:500–516, 2010.

[14]Reiner, B. I. N., N. Knight, and E. L. Siegel. Radiology reporting, past, present, and future: the radiologist's perspective. *J. Am. Coll. Radiol.* 4:313–319, 2007.

[15]Ren, N., J. Liang, X. Qu, J. Li, B. Lu, and J. Tian. GPU-based Monte Carlo simulation for light propagation in complex heterogeneous tissues. *Opt. Express.* 18:6811–6823, 2010.

[16]Robertson, R., M. S. Germannos, C. Li, G. S. Mitchell, S. R. Cherry, and M. D. Silva. Optical imaging of Cerenkov light generation from positron-emitting radiotracers. *Phys. Med. Biol.* 54:N355–N365, 2009.

[17]Ruggiero, A., J. P. Holland, J. S. Lewis, and J. Grimm. Cerenkov luminescence imaging of medical isotopes. *J. Nucl. Med.* 51:1123–1130, 2010.

[18]Spinelli, A. E., D. D'Ambrosio, L. Calderan, M. Marengo, A. Sbarbati, and F. Boschi. Cerenkov radiation allows in vivo optical imaging of positron emitting radiotracers. *Phys. Med. Biol.* 55:483–495, 2010.

[19]Tian, J., J. Bai, X. Yan, S. Bao, Y. Li, W. Liang, and X. Yang. Multimodality molecular imaging. *IEEE Eng. Med. Biol. Mag.* 27:48–57, 2008.

[20]Zhao, H., F. Gao, Y. Tanikawa, and Y. Yamada. Time-resolved diffuse optical tomography and its application to in vitro and in vivo imaging. *J. Biomed. Opt.* 12:062107, 2007.

[21]Zhu, S., J. Tian, G. Yan, C. Qin, and J. Feng. Cone beam micro-CT system for small animal imaging and performance evaluation. *Int. J. Biomed. Imaging* 2009:960573, 2009.